Ground response to tunnelling incorporating a soil reinforcement system

Authors:
Binh Thanh Le, BSc PhD
Ho Chi Minh City University of Transport, Vietnam
Formerly City, University of London, London, UK
School of Mathematics, Computer Science & Engineering, Civil Engineering
binhle@city.ac.uk

R N Taylor, MA PhD CEng MICE
City, University of London, London, UK
School of Mathematics, Computer Science & Engineering, Civil Engineering
R.N.Taylor@city.ac.uk

Corresponding Author's Name: Binh Thanh Le

Abstract

The Forepole Umbrella System (FUS) uses steel pipes installed from within a tunnel to provide a canopy above the tunnel heading that both increases stability and reduces tunnelling-induced ground movements. Although the system is known to be beneficial and has been used in a number of projects, there is little information on how key parameters including length and forepole stiffness combine to produce effective support. To investigate this, centrifuge tests incorporating the three-dimensional geometry of a tunnel heading in clay and the model FUS have been undertaken. The tunnel heading was supported by a pressurised rubber bag lining with excavation being simulated by a reduction in air support pressure. Image analysis was used to obtain subsurface ground movements and a newly developed 3D imaging system was used to measure accurately the soil surface deformations. The performance of the FUS and the influences of key FUS parameters were quantified via the settlement reduction factor. The results showed that the FUS, arranged in various settings, reduced the maximum surface settlement by 35-75%. The effects of the FUS parameters to the reinforcing effectiveness is dependent on the ratio of cover depth to tunnel diameter. An optimum design arrangement of the FUS is suggested.

Keywords: **Centrifuge modelling; Ground improvement; Tunnels & tunnelling;**

LIST OF SYMBOLS

3D	three-dimensional
3DIS	three-dimensional imaging system
C	cover depth above tunnel
D	tunnel diameter
E	Young's modulus of model forepoles
FUS	Forepoling Umbrella System
g	acceleration due to gravity (9.81m/s^2)
P	unlined portion of tunnel heading
PIV	Particle Image Velocity
SRF	settlement reduction factor
u	horizontal displacement in X direction
v	horizontal displacement in Y direction
w	vertical displacement in Z direction
z	depth from soil surface
α	filling angle
σ_T	tunnel support pressure
σ_{ob}	overburden stress at tunnel centreline
σ'_{v0}	consolidation pressure

INTRODUCTION

The reinforcing effectiveness of a Forepoling Umbrella System (FUS) on soil deformations due to open-face tunnelling in clay can be investigated using physical modelling techniques. A FUS consists of steel pipes (forepoles) installed in a canopy shape ahead of an advancing tunnel (**Fig. 1)** to provide structural support to the surrounding soil. As an in-tunnel measure, one of the noticeable advantages of the FUS is the immediate support from the steel pipes to reduce soil deformations at their source.

Fig. 2 illustrates a schematic diagram of a FUS and defines the main parameters of the system and a tunnel heading. The steel pipes with length L are normally inserted into the ground from within the tunnel at an insertion angle β. The steel pipes are arranged along the perimeter of the upper part of the tunnel in a filling angle α. The tunnel lining and the soil beneath the embedded length, *EL*, both act like foundations to support the steel pipes that bridge over the unlined tunnel heading P. The embedded length is supported by the so-called foundation effect ahead of the tunnel face as illustrated in **Fig. 2**. The foundation effect depends on the stiffness of tunnel lining and the undrained shear strength of soil beneath the forepoles. Case histories have demonstrated that FUS are suitable for use in a variety of ground conditions that can provide a sufficiently competent foundation effect for the forepoles such as clay (Gall and Zeidler 2008), mixed soil comprising boulders in hard sandy silt or sandy silty clay matrix (Yeo et al. 2009), claystone, mudstone and sandstone (Volkmann and Schubert 2007; Aksoy and Onargan 2010), low to medium plasticity silty clay (Wang et al. 2018), rocks (Oke 2016), sandstone–siltstone–claystone–shale sequences, gravel–sand–silt, clay-marl, limestone with shale (Ocak 2008).

The common parameters of a FUS in practice are presented in **Table 1** (Volkmann and Schubert 2007). Note that in this paper, the normalised tunnel depth is represented by the dimensionless cover to diameter ratio C/D.

The FUS has been shown to be an efficient measure to control soil deformations due to open face tunnelling and has been used in a number of major projects such as the Victoria Station Upgrade and King’s Cross Station Redevelopment in the UK (Gall and Zeidler 2008), the Harbin

Metro Line #1 in China (Wang et al. 2018), the Istanbul Metro in Turkey (Ocak 2008), and the Fort Canning Tunnel in Singapore (Yeo et al. 2009). Field measurements and numerical analysis reported Oke (2016) showed that the Forepole Umbrella System, when used in conjunction with other soil reinforcement measures (including face bolts and soil nails), provided a reduction of approximately 20-76% surface settlement compared with the unreinforced sections. Similar to the observations made by Oke (2016), Ocak (2008) reported that the combination of several soil reinforcement measures, umbrella arch and soil nailing, reduced the magnitude of surface settlement by three compared with that in the section without soil reinforcement. However, because of the interaction of the various reinforcing techniques used, it is not possible to identify the exact contribution made by the Forepoling Umbrella System in reducing ground movements.

Although previous research has reported on the effects of the FUS, there are still limitations in understanding the influence of the FUS parameters, including forepole stiffness, EL, and α, on the reinforcement effectiveness of the system.

Vrba and Barták (2007) used centrifuge modelling to study the effects of a FUS for a tunnel at a normalised depth C/D=3. In their experiments, steel plates were used to model the forepoling roof which reinforced the tunnel heading in clay. They observed significant reduction in soil settlement was provided by using the FUS. Divall et al. (2016) conducted centrifuge tests simulating a tunnel in clay incorporating a FUS in which the forepoles were modelled by resin. The normalised tunnel depth was C/D=2. Similar to the observations made by Vrba and Barták (2007), Divall et al. (2016) showed that the use of the FUS increased the stability of the tunnel heading and decreased the magnitude of soil settlement. It should be noted that in each research project, the material and geometry of the model forepoles was not varied. The effect of the forepole stiffness was therefore not investigated.

Volkmann and Schubert (2007) reported field measurements obtained from an inclinometer chain located on the topmost steel pipe of the FUS in the Trojane tunnel (Slovenia). The site geology consisted of faulted mudstone, claystone and sandstone (Volkmann et al. 2006). The normalised tunnel depth was C/D=1.5. The measurement data showed that when the embedded length *EL* decreased, as the tunnel face advanced, the magnitude of steel pipe deformation increased. The reason was that when *EL* reduced, the foundation effect from the ground beneath the FUS decreased which led to large deformation of the forepoles. This confirmed similar findings derived from centrifuge tests reported by Vrba and Barták (2007) and Yeo (2011).

The variations in the insertion angle, β, only caused slight differences in soil settlement as noted by Eclaircy-Caudon et al. (2006) and hence β is not considered as a key parameter of the FUS and will not be investigated in this study. The effect of the filling angle α was investigated in a series of plane strain centrifuge tests conducted by Divall et al. (2016). By adopting a 2D modelling approach, this work was able to determine the effect of α independently from the unsupported length *P* and the embedded length *EL*. The test results showed that having the forepoles distributed down to the tunnel springline or even lower can be beneficial for reducing soil deformations and increasing tunnel stability. They concluded that tunnel stability was improved by positioning reinforcement to prevent the development of the plastic collapse mechanisms proposed by Davis et al. (1980).

Davis et al. (1980) suggested that C/D governs soil deformation mechanisms. Therefore, the reinforcement effectiveness of the FUS in reducing soil movements is expected to vary at different C/D. Thus, the influence of C/D on the effect of the FUS is an important factor that needs to be investigated.

THE CENTRIFUGE TESTS

Test series

The centrifuge test variables, including C/D, material of the model forepole, EL and α, were chosen so as to obtain a clearer insight into an optimal design of the FUS.

The normalised depths of C/D=1 and C/D=3 were chosen because these two are likely to result in substantial differences in the soil deformation mechanism (Davis et al. 1979) which is an important factor that influences the reinforcement effectiveness of the FUS (Le and Taylor 2017).

In practice, typical filling angle ranges from α=60° to α=75°. Yeo (2011) and Le (2017) showed that even in a shallow tunnel (C/D=1), there were noticeable soil displacements above the tunnel spring line. Therefore, in the model tests, a filling angle smaller than 75° was not chosen and instead α=75° and α=90° are used to assess the effect of the filling angle.

Fig. 3 presents the variables of the centrifuge experiments that comprise reference tests (no FUS) and tests incorporating a FUS. The identities indicate the variables as explained below:

- CD1 or CD3 denotes the normalised depth of the tunnel C/D=1 or C/D=3;
- R or F denotes reference test (no forepoles) or test incorporating a FUS;
- B or S denotes the model forepole material, brass or steel;
- EL0.5 or EL1 denotes the embedded length EL/D=0.5 or EL/D=1.
- A75 or A90 denotes the value of filling angle α=75° or α=90°;
- N denotes that soil deformations were measured using the new 3D imaging system (Le et al. 2016).

All tests were conducted using the apparatus and procedures outlined below.

Test apparatus

A schematic of the centrifuge model is illustrated in **Fig. 4**. The model clay (Speswhite kaolin) was one dimensionally consolidated in a model container (strong box) using a hydraulic consolidometer to a vertical effective stress σ'_{v0}=175kPa. The consolidation pressure σ'_{v0}=175kPa was chosen as it provided a soft clay model in which the soil deformations, induced by the simulated tunnel excavation, would be sufficiently large so that the reinforcement effects of the FUS would be observed clearly. The properties of Speswhite kaolin are presented in **Table 2** (Le 2017)

The tunnel was simulated by a semi-circular cavity cut into the clay model (**Fig. 4**). By doing so, soil deformations on the vertical plane of symmetry of the tunnel heading could be observed through the front perspex window. The total length of the tunnel cavity was 190mm. This was partially supported by a 165mm long tunnel lining made from a 50mm diameter 1.6mm thick semi-circular stainless steel tube. The unlined heading of length P=25mm was supported by a thin rubber bag supplied with compressed air pressure. The technique of using a pressurised air bag has been proved to be a successful method capable for simulating tunnel excavation in centrifuge models and the soil movements in 3D models were found to be consistent with those obtained from field measurements (Meguid et al. 2008; Le and Taylor 2018).

For each reinforced test, a total of fourteen 1mm diameter rods (brass or steel) were used to model the forepoles. The length of the rods, L, was 100mm. The model forepoles were inserted around the tunnel heading via a guide produced by precision 3D printing (**Fig 5**).

All the tests were conducted at 125*g*. Applying the normal centrifuge scaling laws to the model then gives the prototype scenario described in **Table 3**. The 1mm diameter brass (or steel) rods under 125*g* have an equivalent bending stiffness as steel pipes of 135mm (or 165mm) outer diameter with an 8mm wall thickness at prototype scale (Le 2017). These sizes of forepoles are common in practice (**Table 1**).

Instrumentation

In most of the tests, surface settlement was measured by a row of displacement transducers using the principles of a Linear Variable Differential Transformer (LVDT), placed along the tunnel centreline, and the Visimet software (Grant 1998) was used to measure soil displacements at the front face of the model from images captured from the font facing camera shown in **Fig. 4**. In the tests CD3-R-N, CD3-F-S-EL0.5-A90-N, and CD3-F-S-EL0.5-A75-N the new 3D imaging system (Le et al. 2016) was used to measure 3D soil displacements at the model surface while GeoPIV_RG (Stanier et al. 2015) was used to measure subsurface soil movements at the front face of the model from the camera images.

The precision of 3DIS (Le et al. 2016) was shown to be within 50μm. Grant (1998) reported that the precision of Visimet was in range of 70-80μm. GeoPIV_RG was reported to have comparable measurement precision with the LVDTs (Stanier et al. 2015).

The high measurement precision offered by the imaging techniques mentioned above indicates that there is a small inherent component of friction at the interface between the Perspex window and the soil model that may affect the soil deformation mechanism. However, consistent with previous authors (Grant 1998; Divall 2013; and Le 2017) it was found that once the soil at the interface moved after overcoming the friction, it continued to displace at the same rate as the rest of the model. In addition, considerable effort was made during the model preparation to minimise the effects of this friction by using both a consistent volume of grease at the Perspex window and volume of texture material placed at the front face of the soil models (Le 2017). As a consequence, the friction at the interface was minimised and had negligible effects on the development of soil displacements in the centrifuge tests. Therefore, the displacement measurement systems used in this research are able to quantify the effects of the FUS parameters.

Two Pore Pressure Transducers (PPTs) model PDCR81 supplied by Druck Limited, Leicester, were installed within the soil model to measure the changes in pore pressure. The purpose of the transducers was to indicate when pore pressure equilibrium had been achieved in the model during centrifuge flight. These PPTs were positioned far away from the tunnel heading to minimise any effects on soil deformations induced by the simulated excavation. The air support pressure in the tunnel bag at the tunnel axis level was measured by a pressure transducer model PX600-200GV series supplied by Omega Engineering Ltd.

Test procedure

The models were accelerated to 125*g* while simultaneously increasing the air pressure inside the tunnel bag, σ_T, to support the overburden stress at the corresponding centrifuge acceleration. The centrifuge was left running until the excess pore pressure dissipated and the clay had reached effective stress equilibrium. The tunnel excavation process was then simulated by gradually reducing the tunnel support pressure σ_T to zero. Data relating to the tunnel support pressure σ_T, LVDT readings and deformations of the clay model were recorded at 1 second intervals for later analysis.

From the in-flight images, it was noticed that the tunnel lining deflected when the tunnel support pressure reduced to 55kPa and 180kPa in tests with tunnel having C/D=1 and C/D=3, respectively. This was owing to the lack of hoop stiffness of the tunnel lining. The initial σ_T was chosen to support the overburden stress near the tunnel centre-line which meant the upper part of the tunnel was over pressurised. When the tunnel pressure was increased the lining initially elongated on its vertical diameter. When the support pressure was reduced, the lining sprang back elastically to its normal shape which caused the ground above the tunnel lining to settle (Le 2017). Therefore, in order to study the effect of FUS on the ground deformations independently from deflection of the stiff lining, the results will be examined as the tunnel support pressure is reduced from σ_T =55kPa for C/D=1 tests and σ_T=180kPa for *C/D*=3.

RESULTS

Some of the results in this research have been reported by Le et al. (2015), Le and Taylor (2016), and Le and Taylor (2017). This section further analyses the test results to provide a clearer and broader insight on the relative effects of the FUS parameters to its reinforcing effectiveness.

The effect of using the FUS

Fig. 6 compares typical subsurface soil deformations and engineering shear strains, when σ_T was reduced to 80kPa, in the reference test CD3-R-N (dashed lines) and the reinforced test CD3-F-S-EL0.5-A75-N (solid lines) to examine the effect of using the FUS. The pressure σ_T=80kPa was chosen because at this pressure soil deformations were large enough so that the effects of the FUS can be observed clearly.

Using a FUS led to a reduction in both magnitude and extent of the soil displacements and shear strains (**Fig. 6**). In the reference test, large engineering shear strains (>4%) developed at both the tunnel crown and invert. In contrast, in the test with the FUS, large shear strains did not occur near the tunnel crown in the vicinity of the FUS. The reduction in soil movements near the tunnel heading, delivered by the FUS, led to a reduction in ground movements in all directions at all points at the entire top surface of the model (**Fig. 7)**.

The maximum surface settlement is of great interest as it indicates the potential damage to near surface structures. **Fig. 8** compares the maximum surface settlement above the tunnel face in the centrifuge tests and highlights the significant reduction in settlement delivered by the FUS. In order to quantify the reinforcing effectiveness of the FUS, the settlement reduction factor (SRF) defined by **Equation 1** is presented in **Fig. 9**;

$$SRF = \left[(w_0 - w_r)/w_0\right] \times 100\% \qquad (1)$$

where w_0, w_r are respectively the maximum surface settlement in the reference and reinforced test with the same geometry and having the same tunnel support pressure;

The SRF is the settlement reduction factor (%), based on a comparison of the maximum surface settlement in the reinforced and reference tests.

It can be seen that the SRF increased when σ_T decreased (**Fig. 9**). This is because initially the overburden pressure, σ_{ob}, was supported by the tunnel support pressure σ_T. As σ_T was reduced, so the stress difference ($\sigma_{ob} - \sigma_T$) was supported by the surrounding soil and the FUS. Thus, the SRF became higher as the stress difference (σ_{ob}–σ_T) increased as a result of the reduction of tunnel support pressure σ_T. The average values of *SRF*, at different σ_T determined from **Fig. 9,** are tabulated in **Table 4** and will be used to examine the reinforcing effectiveness of the FUS for different arrangements. The average values were used so as to be representative for the entire test.

RELATIVE INFLUENCE OF THE FUS PARAMETERS

The same pre-consolidation pressure was used for the clay models and hence all the models had similar strength and stiffness characteristics. Therefore, any significant differences in the reinforcement effectiveness of the FUS were the result of the variation of the arrangement including *EL/D*, α, material of the forepoles and C/D ratios which are discussed in detail in the following sections.

Effect of EL/D with different C/D

The influence of *EL/D* on the *SRF* of the FUS is tabulated in **Table 5**. Generally, increasing the embedded length offered a greater foundation effect to the FUS which resulted in a greater *SRF*. It is worth noting that besides *EL/D*, there are other differences between the tests in this section including the starting point of the FUS and the radial distance from the modelled forepoles to the tunnel lining. However, the effects of these differences are negligible because the performance of the FUS is mainly dependent on the foundation effects provided by the two components: the tunnel lining, which is the same for all the tests; and the surrounding soil, which is dictated by *EL/D*. Therefore, it can be argued that the differences in the soil deformations observed in these tests were mainly due to the variation of *EL/D*.

The difference in the foundation effect between *EL*/*D*=0.5 and *EL*/*D*=1 to the FUS was reflected in the corresponding deformation of the forepoles as shown in **Fig. 10**. The model rods for the *EL*/*D*=0.5 test showed one inflexion point implying that the foundation effect was negligible and that the forepoles worked mainly as a cantilever. In contrast, the rods for *EL*/*D*=1 test showed two inflexion points denoting that the foundation effect was greater and the forepoles worked like beams supported at both ends and this offered a better supporting effect.

For the *C*/*D*=3 tunnels, increasing *EL/D* by 100% (from *EL*/*D*=0.5 to *EL*/*D*=1) gave a 10% increase in SRF (CD3-F-B-EL0.5-A90 vs CD3-F-B-EL1-A90; CD3-F-S-EL0.5-A90 vs CD3-F-S-EL1-A90, see **Table 5**). Interestingly, for the *C*/*D*=1 tunnels (CD1-F-B-EL0.5-A90 vs CD1-F-B-EL1-A90), the same increase in *EL*/*D* gave an increase of 29% in SRF which is approximately 3 times larger than that for the C/D=3 tunnels. This significant difference in the influence of *EL/D* to the reinforcing effectiveness of the FUS for the two normalised tunnel depths suggests that the quality of the foundation effect provided by the soil beneath the FUS was different.

Figs. 11a and 11b present photographs of the reference tests having *C*/*D*=1 and *C*/*D*=3 respectively. The failure planes observed in these tests are highlighted by dashed lines. The pictures are further annotated with the outline of a potential upper bound failure mechanism suggested by Davis et al. (1980). The angles in the failure mechanism are given by;

$$\tan\theta_1 = \tan\theta_2 = 2\sqrt{C/D + 1/4} \qquad (2)$$

$$\theta_3 = \pi/2 \qquad (3)$$

(θ_1, θ_2 and θ_3 are annotated in **Fig. 11**)

It can be seen that the upper bound mechanisms over predict the extent of the collapse zones for both tests which may reflect the fact that the upper bound mechanism is for a plane strain tunnel (long wall mining) rather than the 3D circular tunnel heading in the centrifuge tests. By way of illustration, the locations of forepoles in a FUS having *EL*/*D*=1 are superimposed on **Fig. 11**. This demonstrates that for *EL/D=1*, the forepoles in a *C*/*D*=1 tunnel extend beyond the shear plane (and plastic collapse mechanism) which then offers a better foundation effect compared with that for a *C*/*D*=3 tunnel where the forepoles would be inside the shearing plane. This better foundation effect may explain the higher SRF of the FUS in the shallow tunnel tests.

These observations provide a clearer insight into the effect of the embedded length *EL* to the foundation effect and the reinforcing effectiveness of the FUS. The foundation effects depend not only on *EL* but also on the magnitude and extent of the soil deformations beneath the FUS. The implication is that the forepoles should extend beyond the expected plastic collapse mechanism which can be estimated by the simple upper bound solutions of Davis et al. (1980).

The effect of the filling angle α for different C/D

It is worth noting that, in this study, varying the filling angle α alters the spacing *S* between the forepoles as the quantity of the forepoles in the reinforced tests is constant. The test results presented later in this section highlighted that at different C/D ratios, the SRF delivered by the FUS heavily depends on the coverage of the forepoles in the transverse direction which is dictated by α. Therefore, the filling angle is chosen as the key parameter for consideration, not the spacing *S.*

Table 6 presents the *SRF* of the FUS for two filling angles α=75° and α=90° at two different normalised tunnel depths *C*/*D*=1 and *C*/*D*=3. The filling angle α=75° outperformed α=90° for tests with *C*/*D*=1 (CD1-F-B-EL0.5-A75 vs CD1-F-B-EL0.5-A90) but not for tests with *C*/*D*=3 (CD3-F-B-EL0.5-A75 vs CD3-F-B-EL0.5-A90; CD3-F-S-EL0.5-A75 vs CD3-F-S-EL0.5-A90).

A photograph of the tunnel heading post-test with the deformed forepoles in test CD1-F-B-EL0.5-A90 (*C*/*D*=1) is presented in **Fig. 12-a**. The upper rods had large deformations while the deformations of the lower rods were negligible. This suggests that large soil movements occurred mainly in the vicinity of the tunnel crown while near the tunnel spring line the soil displacement was small. This agrees with the collapse mechanism A suggested by Davis et al. (1980) for a shallow tunnel (**Fig. 12-b**). Therefore, concentrating forepoles near the tunnel crown by arranging the same quantity of forepoles within a filling angle of α=75° outperformed α=90° by ≈10% in terms of *SRF* (**Table 6**).

For the *C*/*D*=3 tunnel (test CD3-F-B-EL0.5-A90), **Fig. 13-a** shows large deformations in both the upper and lower forepoles which implies that large soil displacements occurred at both the tunnel crown and near the tunnel spring line. This is relevant to the tunnel collapse mechanism D suggested by Davis et al. (1980) for a tunnel with larger *C*/*D* (**Fig. 13-b**). Hence, arranging the same quantity of forepoles in α=90°, instead of α=75°, provided more forepoles near the tunnel spring line, where large lateral soil displacements occurred, and this resulted in a better *SRF*.

The effect of the forepole stiffness

Generally, for the same arrangement of forepoles, an increase in the forepole stiffness led to a higher *SRF* as shown in **Table 7**.

The increase in *SRF* offered by increasing the forepole stiffness (brass to steel) for *C*/*D*=1 tunnel was ≈30% (α=75°) which is more significant than that for the *C*/*D*=3 tunnels which showed increases of approximately 10% and 20% for α=75° and α=90° respectively.

Interestingly, for *C*/*D*=3 tests increasing the forepoles stiffness yielded different improved *SRF* for different filling angles α. In tests with forepoles arranged at α=90° ([CD3-F-B-EL1-A90 vs CD3-F-S-EL1-A90]; [CD3-F-B-EL0.5-A90 vs CD3-F-S-EL0.5-A90-N]), the stiffness increase delivered an increase of approximately 20% in *SRF* (**Table 7**). This is about two times larger than the 10% increase in *SRF* for tests with α=75° (CD3-F-B-EL0.5-A75 vs CD3-F-S-EL0.5-A75-N) (**Table 7**) which suggests that the benefit of increasing in the forepole stiffness can be maximised if the forepoles are arranged at an appropriate filling angle.

It can also be noted that by only increasing the forepole stiffness, the measured *SRF* was similar to that achieved by increasing the embedded length (from *EL*/*D*=0.5 to *EL*/*D*=1) for *C*/*D*=1 tunnels (test CD1-F-S-EL0.5-A90 vs CD1-F-B-EL1-A90, see **Table 4**). A practical application for this observation is that using forepoles with higher stiffness requires a lower EL/D and this then permits a longer excavation length which could be beneficial in terms of time saving.

SUMMARY AND CONCLUSIONS

The series of centrifuge tests has investigated of the effects of a FUS in reducing ground movements around a tunnel heading. Data of subsurface and surface ground movements has demonstrated the benefits of using a FUS in reducing the magnitude and extent of soil deformations. The high precision measurements, including those from a novel 3D imaging system in some centrifuge tests, allowed the reinforcing effect of the FUS to be quantified and a more detailed analysis of 3D displacements at the surface to be made than has previously been possible.

The deformed model forepoles recovered after the tests revealed information on patterns and zones of movements. In the longitudinal direction, the forepoles were found to be most effective when able to mobilise a “foundation effect” at the end of the forepoles furthest from tunnel. This requires the forepoles to extend beyond the potential plastic collapse mechanism. The potential failure mechanism can be predicted using simple upper bound solutions for a plane strain heading suggested by Davis et al. (1980).

In the transverse direction, the experimental evidence further corroborates the Davis et al. (1980) plastic failure mechanisms which suggests increased likelihood of lateral movements near the tunnel springline as *C/D* increases. Therefore, the forepoles need to extend around the tunnel periphery into areas where significant soil movements might be expected from consideration of the plastic failure mechanism. Further studies with an α>90° would be needed to investigate the effect of larger filling angle on the reinforcement effectiveness of the FUS for deep tunnels.

The key findings can be summarised by **Fig. 14** which demonstrates the *SRF* (from **Table 4**) for different ratios of *EL*/*D* and *C*/*D* and also for changing the stiffness of the forepoles. This chart would be useful as a guide for designing the FUS in practice.

Acknowledgements

The first author acknowledges the Vietnam government for funding his doctoral scholarship. The authors are grateful to colleagues in the Research Centre for Multi-scale Geotechnical Engineering at City, University of London for their support.

REFERENCES

Aksoy, C.O. and Onargan, T. 2010. The role of umbrella arch and face bolt as deformation preventing support system in preventing building damages. Tunnelling and Underground Space Technology 25 (5), 553–559.

Carrieri, G., Fiorotto, R., Grasso, P. and Pelizza, S. 2002. Twenty years of experience in the use of the umbrella-arch method of support for tunnelling. Proc. 4th Int. Workshop on Micropiles, Venice.

Divall, S. 2013. Ground movements associated with twin-tunnel construction in clay. PhD thesis, City, University of London, UK.

Divall, S., Taylor, R. N. and Xu, M. 2016. Centrifuge modelling of tunnelling with forepoling. International Journal of Physical Modelling in Geotechnics, doi: 10.1680/jphmg.15.00019

Davis, E.H., Gunn, M.J., Mair, R.J. and Seneviratine, H.N. 1980. The stability of shallow tunnels and underground openings in cohesive material. Geotechnique, 30(4), pp.397-416.

Eclaircy-Caudron, S., Disa, D., Kastner, R. and Chantron, L. 2006, March. Numerical modelling of a reinforcement process by umbrella arch. In International Conference on Numerical Simulation of Construction Processes in Geotechnical Engineering for Urban Environment (NSC06), Bochum (Germany).

Gall Zeidler Consultants, L.L.C. and Ashburn, V. 2008. Pre-Support Measures for Shallow NATM Tunneling in Urban Settings. North American Tunneling 2008 Proceedings, p.152.

Grant, R.J. 1998. Movements around tunnel in two-layer ground. PhD thesis, City University London, UK.

Le, B.T. 2017. The effect of forepole reinforcement on tunnelling-induced movements in clay. PhD thesis, City, University of London, UK.

Le, B. T. and Taylor, R.N. 2016. A study on the reinforcing capabilities of Forepoling Umbrella System in urban tunnelling. Paper presented at the The 3rd European Conference on Physical Modelling in Geotechnics, 1-3 Jun 2016, Nantes, France.

Le, B.T. and Taylor, R.N. 2017. The reinforcing effects of Forepoling Umbrella System in soft soil tunnelling. Proceedings of the 19th International Conference on Soil Mechanics and Geotechnical Engineering, pp. 1709-1712.

Le, B.T. and Taylor, R.N. 2018. Response of clay soil to three-dimensional tunnelling simulation in centrifuge models. Soils and Foundations, 58(4), pp. 808-818.

Le, B.T., Divall, S. and Taylor, R.N. 2015. The effect of a forepole umbrella system on the stability of a tunnel face in clay. Proceedings of the XVI ECSMGE Geotechnical Engineering for Infrastructure and Development.

Le, B.T., Nadimi, S., Goodey, R.J. and Taylor, R.N. 2016. System to measure three-dimensional movements in physical models. Géotechnique Letters, 6(4), pp. 256-262.

Meguid, M.A., Saada, O., Nunes, M.A. and Mattar, J. 2008. Physical modeling of tunnels in soft ground: a review. Tunnelling and Underground Space Technology, 23(2), pp.185-198.

Ocak, I. 2008. Control of surface settlements with umbrella arch method in second stage excavations of Istanbul Metro. Tunnelling and Underground Space Technology, 23(6), pp.674-681.

Oke, J.D.S.H. 2016. Determination of nomenclature, mechanistic behaviour, and numerical modelling optimization of umbrella arch systems. PhD Thesis, Queen's University, Canada.

Specification for tunnelling Third edition. 2012. British Tunnelling Society (BTS) & Institution of Civil Engineers (ICE).

Stanier, S.A. Blaber, J., Take, W.A. and White, D.J. 2015. Improved image based deformation measurement for geotechnical applications. Canadian Geotechnical Journal.

Volkmann, G.M. and Schubert, W. 2007, May. Geotechnical model for pipe roof supports in tunneling. In Proceeding of the 33rd ITA-AITES World tunneling congress, underground spaced the 4th dimension of metropolises. London: Taylor & Francis Group (pp. 755-760).

Volkmann G.M., Button E.A. and Schubert W. 2006. A Contribution to the Design of Tunnels Supported by a Pipe Roof. Proc. 41st U.S. Rock Mechanics Symp., American Rock Mech. Assoc., June 17-21, Golden, CO.

Vrba, V. and J. Barták. 2007. Model analysis of pre-lining methods used in tunnel construction. In Proceedings of the World Tunnel Congress 2007 and 33rd ITA/AITES Annual General Assembly, Prague, May 2007.

Wang, Z., Li, W., Li, S., Qiu, W. and Ding, W.. 2018. Development of an Optimum Forepole Spacing (OFS) determination method for tunnelling in silty clay with a case study. Tunnelling and Underground Space Technology, 74, pp.20-32.

Yeo, C.H. 2011. Stability and collapse mechanisms of unreinforced and forepole-reinforced tunnel headings. PhD Thesis, National University of Singapore.

Yeo, C.H., Lee, F.H., Tan, S.C., Hasegawa, O., Suzuki, H. and Shinji, M. 2009. Three dimensional numerical modelling of a NATM tunnel. International Journal of the JCRM, 5(1), pp.33-38.

FIGURE CAPTION

Fig. 1: Forepoling Umbrella System (after Carrieri et al. 2002)

Fig. 2: Parameters in a tunnel heading and a FUS.

Fig. 3: Variables of centrifuge test.

Fig. 4: Schematic of the centrifuge model.

Fig. 5: 3D printed guide for inserting the model forepoles into the clay model during the modelling preparation stage at 1g.

Fig. 6: Subsurface soil deformations in test reference test CD3-R-N and reinforced test CD3-F-S-EL0.5-A75-N ($\sigma_T = 80kPa$).

Fig. 7: Soil displacements at the top of the model in tests CD3-R-N and CD3-F-S-EL0.5-A75-N(mm) ($\sigma_T = 80kPa$).

Fig. 8: Typical maximum surface settlement above tunnel face in centrifuge tests.

Fig. 9: Settlement reduction factor SRF of the FUS in different arrangements.

Fig. 10: Photos of forepoles post-test and associated schematics indicating the position of the points of inflexion relative to the model tunnel.

Fig. 11: Photos of models post-test annotated with the observed failure planes and upper bound failure mechanism.

Fig. 12: Tunnel heading and forepoles post test in test CD1-F-B-EL0.5-A90 (*C*/*D*=1).

Fig. 13: Tunnel heading and forepoles post test in test CD3-F-B-EL0.5-A90 (*C*/*D*=3).

Fig. 14: Relationship between *SRF* and *EL*/*D* with variation of forepole stiffness.

Parameter	Unit	Value
Steel pipe diameter and wall thickness	mm mm	70-200 4-8
Steel pipe length, *L*	m	12-18
Embedded length, *EL*	m	3-6
Insertion angle, β	°	5-7
Filling angle, α	°	60-75

Table 1: Parameters in a FUS (Volkmann and Schubert 2007).

Symbol	Parameter	Value
κ	average gradient of swelling line in v:$\ln p'$ space	0.05
λ	gradient of compression line in v:$\ln p'$ space	0.19
M	stress ratio at critical state (q': p')	0.89
Γ	specific volume at critical state when p'=1kPa	3.23
N	specific volume on INCL when p'=1kPa	3.29
φ'_c	critical state angle of shearing resistance	23°
γ	unit weight of soil (saturated for clay)	16.5 (kN/m^3)
γ_w	unit weight of water	9.81 (kN/m^3)

Table 2. Properties of Speswhite Kaolin (Le 2017).

Parameter	Model (mm)	Prototype (m)
Tunnel Diameter, *D*	50	6.25
Unlined portion, *P*	25	3.125
Cover depth *C* (*C*/*D*=1)	50	6.25
Depth at tunnel CL, z_0 (*C*/*D*=1)	75	9.375
Cover depth *C* (*C*/*D*=3)	150	18.75
Depth at tunnel CL, z_0 (*C*/*D*=3)	175	21.875

Table 3: Corresponding tunnel at prototype scale.

Test	*C*/*D*	Model forepole	*EL*/D	α(°)	*E* (GPa)	*SRF* (%)
CD3-F-B-EL0.5-A75	3	Brass	0.5	75	110	35
CD3-F-B-EL1-A90	3	Brass	1	90	110	50
CD3-F-B-EL0.5-A90	3	Brass	0.5	90	110	42
CD3-F-S-EL1-A90	3	Steel	1	90	210	73
CD3-F-S-EL0.5-A90-N	3	Steel	0.5	90	210	62
CD3-F-S-EL0.5-A75-N	3	Steel	0.5	75	210	47
CD1-F-B-EL0.5-A75	1	Brass	0.5	75	110	53
CD1-F-B-EL0.5-A90	1	Brass	0.5	90	110	44
CD1-F-B-EL1-A90	1	Brass	1	90	110	75
CD1-F-S-EL0.5-A90	1	Steel	0.5	90	210	72

Table 4: Average value of settlement reduction factor SRF.

Tests	C/D	α (°)	Model forepoles	*SRF* (%)		$SRF_{EL/D=1}$ - $SRF_{EL/D=0.5}$ (%)
				EL/*D*=0.5	*EL*/*D*=1	
CD3-F-B-**EL0.5**-A90 vs CD3-F-B-**EL1**-A90	3	90	Brass	42	50	8
CD3-F-S-**EL0.5**-A90 vs CD3-F-S-**EL1**-A90	3	90	Steel	62	73	11
CD1-F-B-**EL0.5**-A90 vs CD1-F-B-**EL1**-A90	1	90	Brass	44	73	29

Table 5: Relative effect of *EL*/*D* with ratio *C*/*D*.

Tests	*C*/*D*	*EL*/*D*	Model forepole	*SRF* (%)		$SRF_{\alpha=90°}$ - $SRF_{\alpha=75°}$ (%)
				α =75°	α =90°	
CD3-F-B-EL0.5-**A75** vs CD3-F-B-EL0.5-**A90**	3	0.5	Brass	35	42	7
CD3-F-S-EL0.5-**A75**-N vs CD3-F-S-EL0.5-**A90**-N	3	0.5	Steel	47	62	15
CD1-F-B-EL0.5-**A75** vs CD1-F-B-EL0.5-**A90**	1	0.5	Brass	53	44	-9

Table 6: Relative effect of filling angle in different ratio *C*/*D*.

Tests	*C*/*D*	α (°)	*EL*/*D*	*SRF* (%)		SRF_{steel} - SRF_{brass} (%)
				Brass	Steel	
CD3-F-**B**-EL0.5-A75 vs CD3-F-**S**-EL0.5-A75-N	3	75	0.5	35	47	12
CD3-F-**B**-EL1-A90 vs CD3-F-**S**-EL1-A90	3	90	1	50	73	23
CD3-F-**B**-EL0.5-A90 vs CD3-F-**S**-EL0.5-A90-N	3	90	0.5	42	62	20
CD1-F-**B**-EL0.5-A90 vs CD1-F-**S**-EL0.5-A90	1	90	0.5	44	72	28

Table 7: Relative effect of filling angle to increase in stiffness of the forepole.

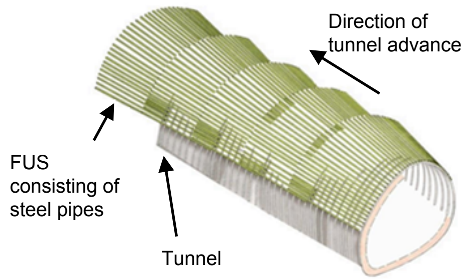

Fig. 1: Forepoling Umbrella System (after Carrieri *et al.* 2002)

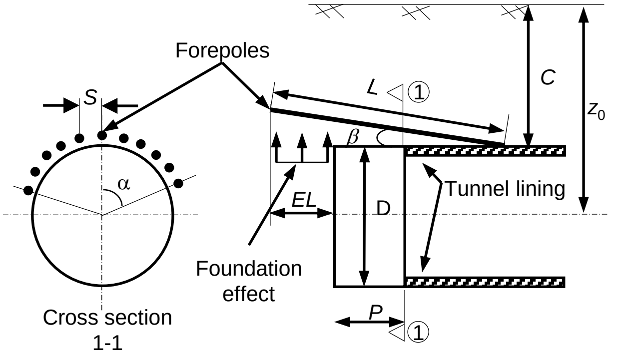

D: tunnel diameter; *C* : cover depth;
P: unlined portion; *EL*: embedded length;
L: forepole length; z_0: tunnel depth
S: centre to centre spacing between forepoles;
β: insertion angle; α: filling angle.

Fig. 2: Parameters in a tunnel heading and a FUS.

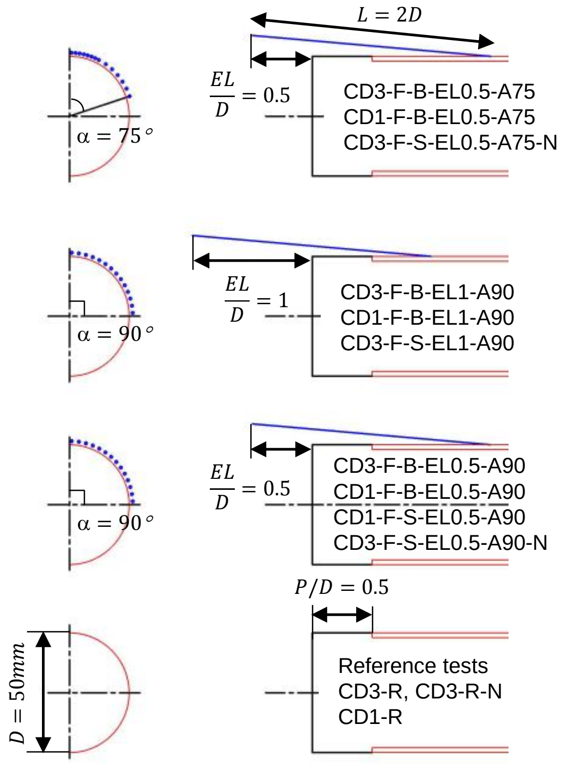

Fig. 3 : Variables of centrifuge tests.

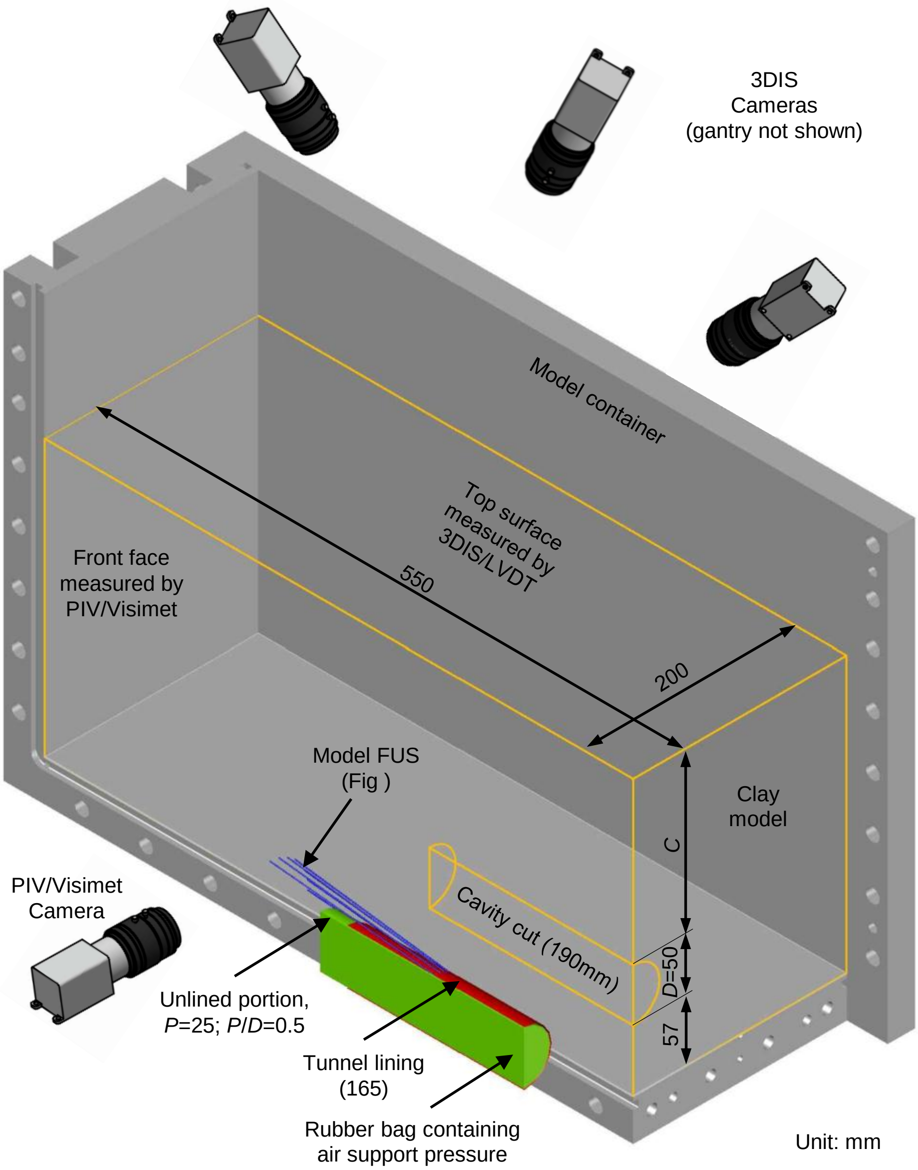

Fig. 4 : Schematic of the centrifuge model.

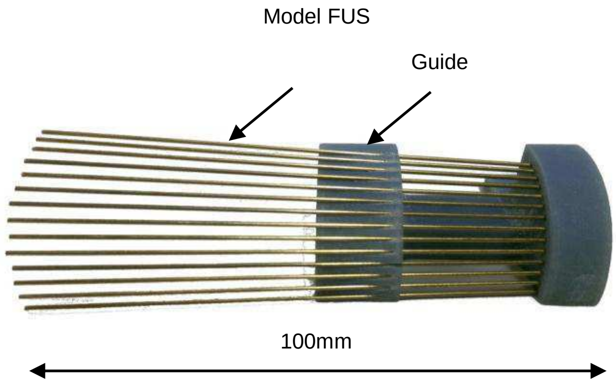

Fig. 5: 3D printed guide for inserting the model forepoles into the clay model during the modelling preparation stage at 1g.

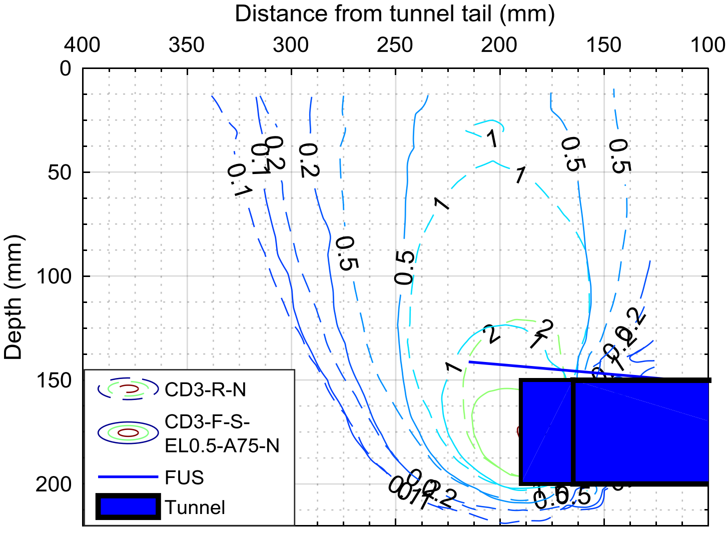

a) Resultant soil displacements (mm).

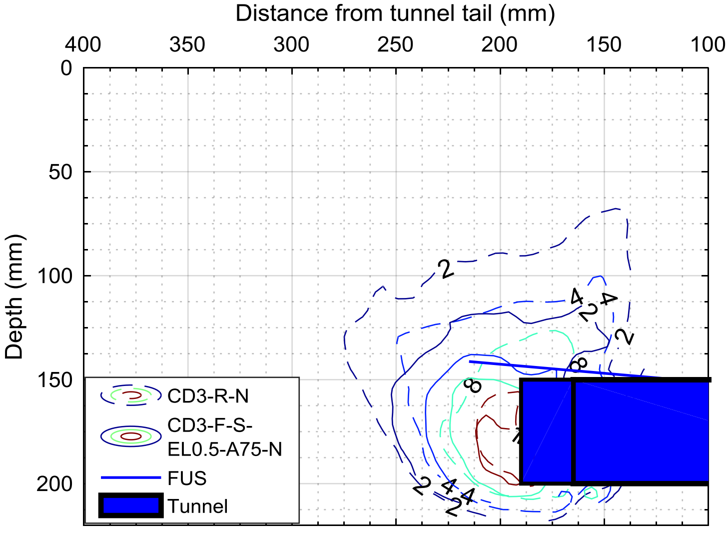

b) Engineering shear strains (%).

Fig. 6: Subsurface soil deformations in test reference test CD3-R-N and reinforced test CD3-F-S-EL0.5-A75-N ($\sigma_T = 80kPa$).

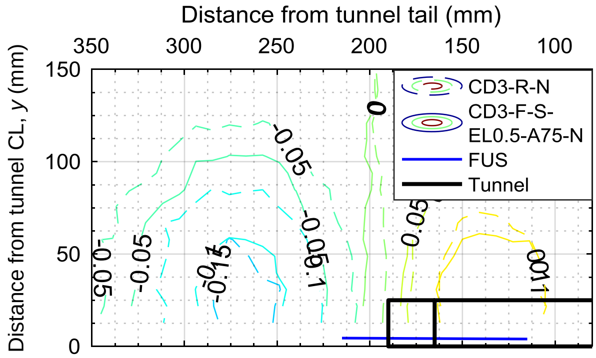

a) Horizontal soil displacements, *u*.

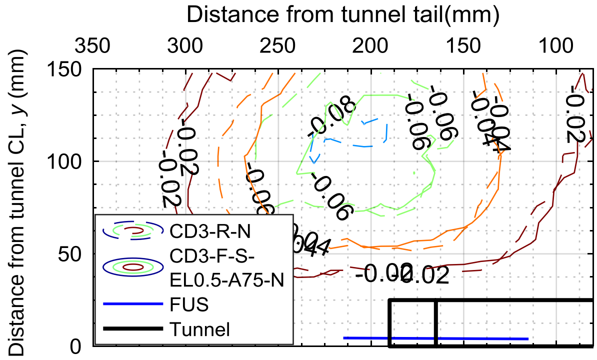

b) Horizontal soil displacements, *v*.

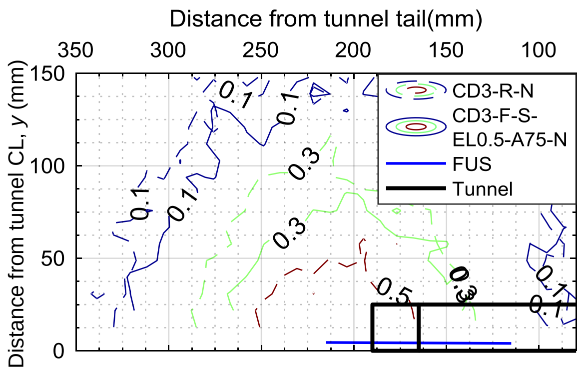

c) Vertical soil displacements, *w*.

Fig. 7: Soil displacements at the top of the model in tests CD3-R-N and CD3-F-S-EL0.5-A75-N(mm) ($\sigma_T = 80kPa$).

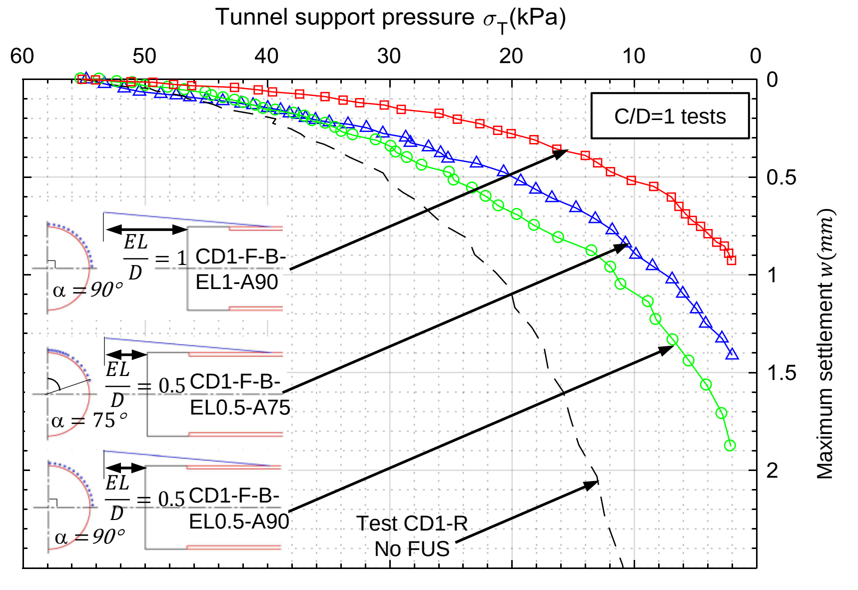

a) In C/D =1 tests.

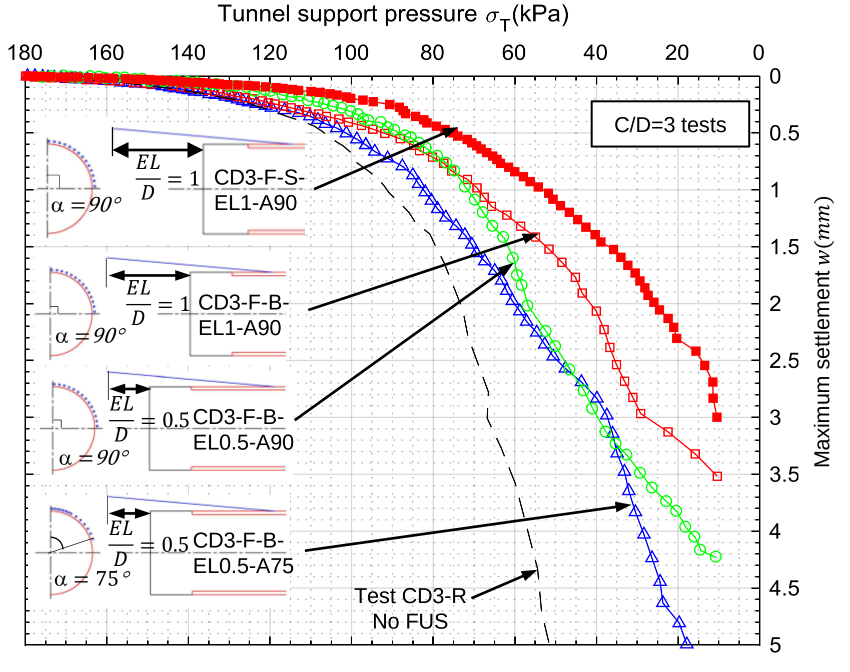

b) In C/D=3 tests.

Fig. 8: Typical maximum surface settlement above tunnel face in centrifuge tests.

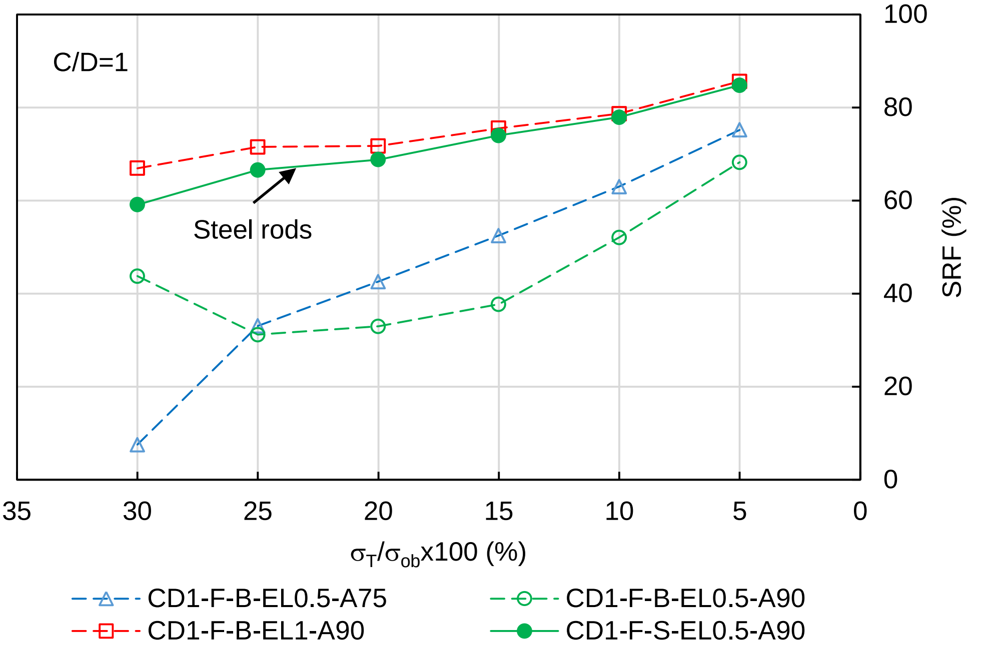

a) In C/D=1 tests

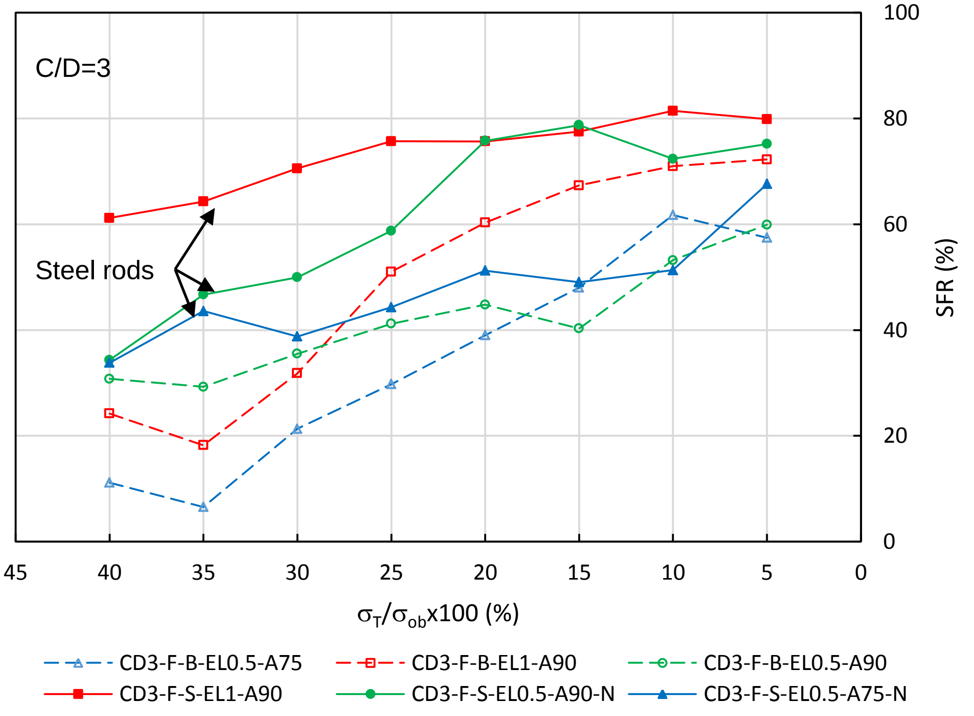

b) In C/D=3 tests

Fig. 9: Settlement reduction factor SRF of the FUS in different arrangements.

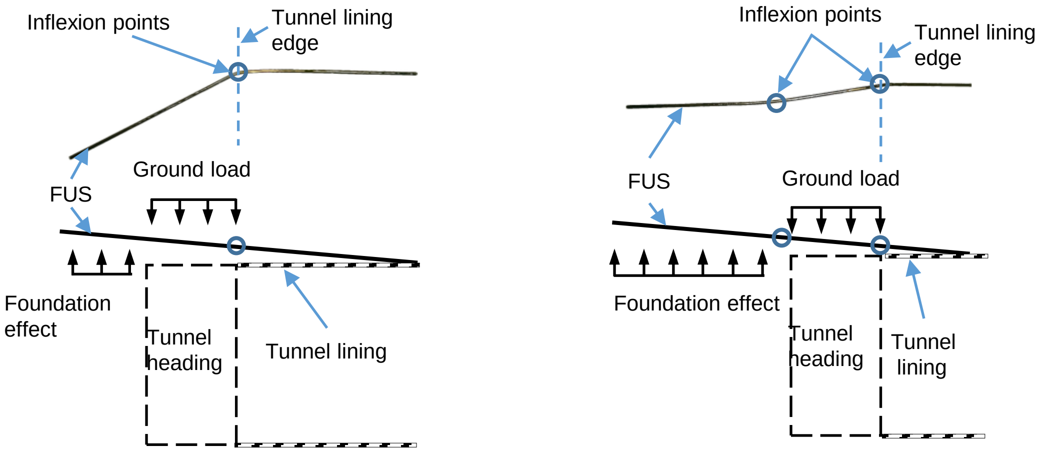

a) Test CD3-F-B-EL0.5-A90

b) CD3-F-B-EL1-A90

Fig. 10: Photos of forepoles post-test and associated schematics indicating the position of the points of inflexion relative to the model tunnel.

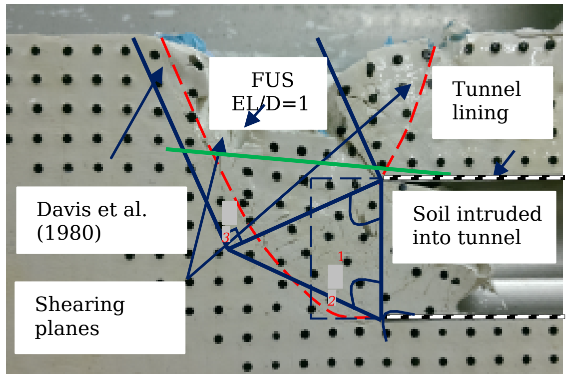

a) Test CD1-R

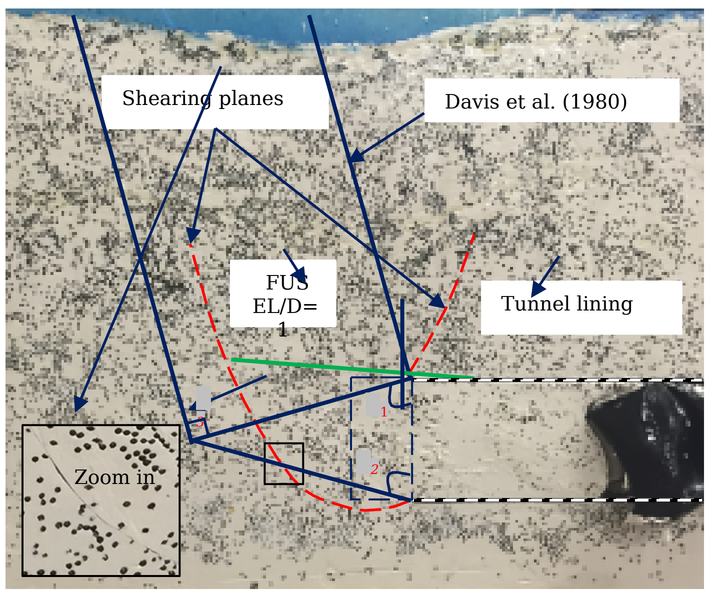

b) Test CD3-R-N

Fig. 11: Photos of models post-test annotated with the observed failure planes and upper bound failure mechanism.

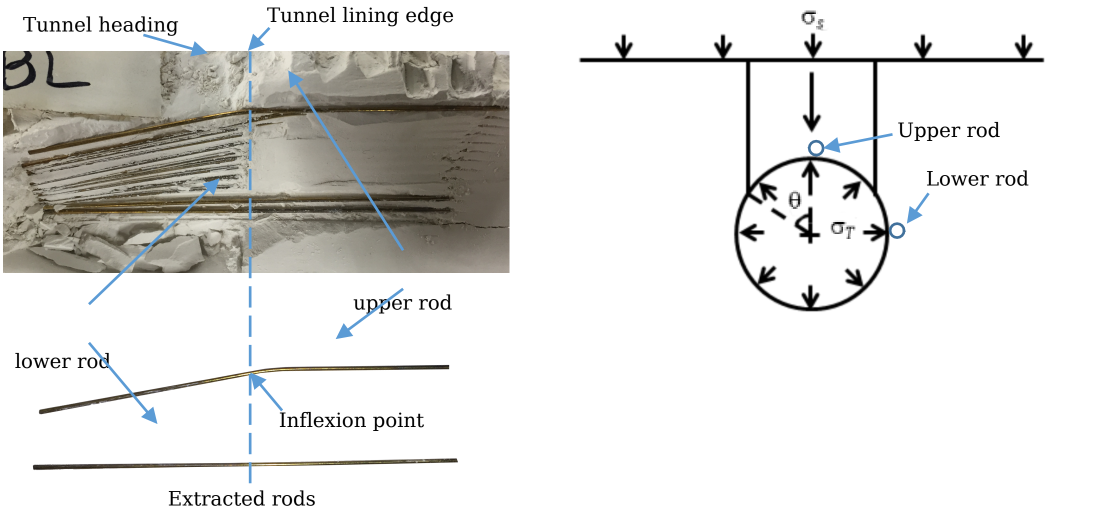

a) Tunnel heading and forepoles post test

b) Upper bound collapse mechanism A for shallow tunnel (after Davis et al. 1980)

Fig. 12: Tunnel heading and forepoles post test in test CD1-F-B-EL0.5-A90 (C/D=1).

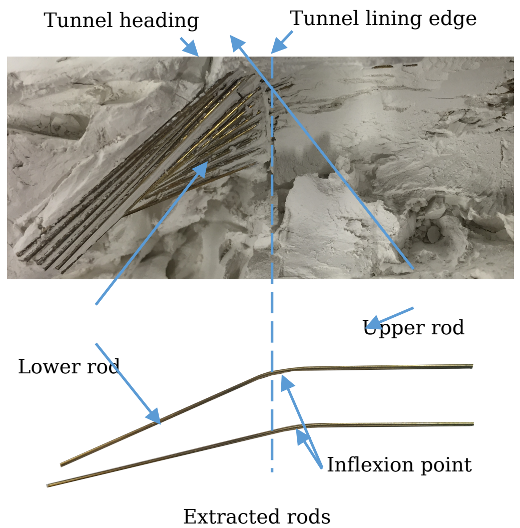

a) Tunnel heading and forepoles post test

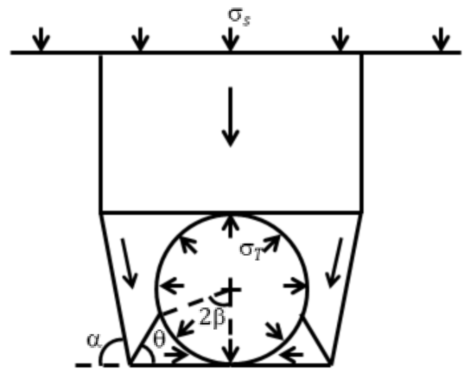

b) Upper bound collapse mechanism D for deep tunnel (after Davis et al. 1980)

Fig. 13: Tunnel heading and forepoles post test in test CD3-F-B-EL0.5-A90 (C/D=3).

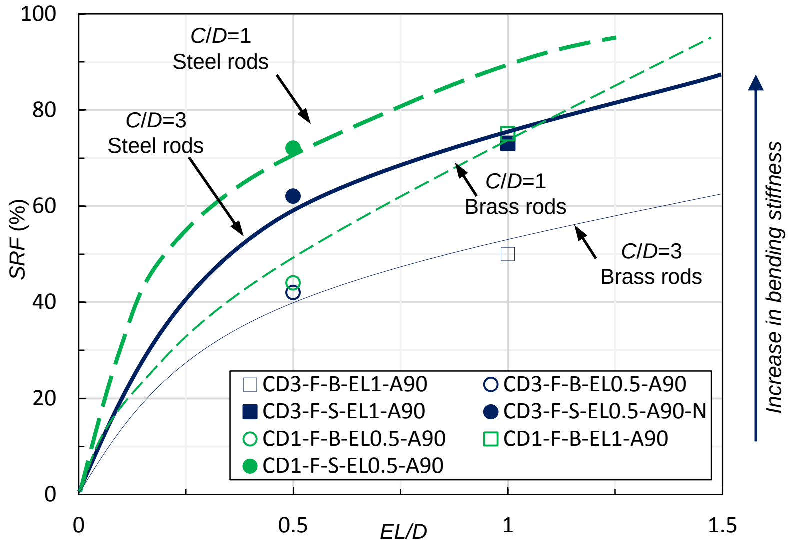

Bending stiffness equivalence:
Brass rod: steel pipes with diameter of 135mm and wall thickness of 8mm
Steel rod: steel pipes with diameter of 165mm and wall thickness of 8mm.

Fig. 14: Relationship between *SRF* and *EL*/*D* with variation of forepole stiffness.